scientific reports

Check for updates

OPEN

TMEM184A promotes progression and drug resistance in colorectal cancer: a bioinformatics and clinical study

Xueliang Bai[1,2], Zhongyuan Bai[4], Peng Bu[2], Ruijiang Liu[1], Guohai Zhao[2], Wei Cui[2], Yongping Cui[3]✉ & Yanfeng Xi[2]✉

The cellular origin and molecular mechanisms underlying therapeutic resistance in colorectal cancer remain largely unclear.This study integrates single-cell transcriptomics, spatial transcriptomics, molecular docking, and multi-cohort public databases to systematically elucidate the epithelial cell-driven drug resistance mechanism, and combines clinical pathological paraffin samples to evaluate the clinical significance and prognosis of the key protein TMEM184A. Integrated single-cell datasets underwent quality control and PCA/UMAP clustering, followed by annotation verified through spatial transcriptomic mapping. CellChat, CopyKat, inferCNV, Monocle3 and AUCell analyses were applied to assess cell–cell communication, CNV heterogeneity and pseudotime differentiation. Integrate the TCGA, GEO data, as well as the drug sensitivity data from GSCA and CTR-DB 2.0, and combine with the AutoDock molecular docking results to explore the correlation between genes and prognosis, as well as immune infiltration, and their pharmacological effects. Use the tissue microarray technique to detect the protein expression of TMEM184A in cancer tissues and adjacent tissues, and analyze its association with clinical pathological features and patient prognosis. The study identified a subset of epithelial cells associated with drug resistance, characterized by the enrichment of interferon, TNF-α/NF-κB, TGF-β, hypoxia, and p53 signaling pathways.By combining machine learning and clinical prognosis analysis, the key drug-resistant driving gene TMEM184A was finally determined. The genes related to TMEM184A were significantly enriched in the lipid metabolism pathway. Moreover, TMEM184A were highly expressed in microsatellite stable colorectal cancer, positively correlated with regulatory T cell (Treg) infiltration, and associated with the "low immune - low stroma" microenvironment. The analysis of immunohistochemical staining on tissue microarrays showed that the high expression of TMEM184A protein was related to lymph node metastasis, and was more prevalent in the rectal region. Additionally, the high expression of TMEM184A was associated with poor prognosis in patients. Drug sensitivity and molecular docking analysis indicated that TMEM184A had strong binding affinity with lapatinib and various EGFR tyrosine kinase inhibitors. TMEM184A promotes the occurrence of drug resistance in colorectal cancer by regulating lipid metabolism. The high expression of this protein in the rectum is more common and is associated with lymph node metastasis and poor prognosis in patients with colorectal cancer. This study provides a theoretical basis for TMEM184A to be used as a prognostic marker and a therapeutic target for drug resistance in colorectal cancer.

Keywords Colorectal cancer, TMEM184A, Drug resistance, Clinical Significance

Abbreviations

CRC	Colorectal cancer
AUCell	Area Under the Curve enrichment scoring

[1]School of Basic Medicine, Shanxi Medical University, Taiyuan 030001, Shanxi, China. [2]Department of Pathology, Shanxi Province Cancer Hospital, Shanxi Hospital Affiliated to Cancer Hospital, Chinese Academy of Medical Sciences, Cancer Hospital Affiliated to Shanxi Medical University, Taiyuan 030013, Shanxi, China. [3]Department of Pathology, Basic Medical Sciences Center, Key Laboratory of Cellular Physiology of Shanxi Medical University, Taiyuan 030001, Shanxi, China. [4]Shanxi Medical University, Taiyuan 030001, Shanxi, China. ✉email: cuiyp@sxmu.edu.cn; xiyanfeng1998@163.com

CAF	Cancer-associated fibroblast
CNV	Copy-number variation
EGFR	Epidermal growth factor receptor
EMT	Epithelial–mesenchymal transition
FDR	False discovery rate
GSEA	Gene set enrichment analysis
ICI	Immune checkpoint inhibitor
MR	Mendelian randomisation
MSS	Microsatellite stable
MSI	Microsatellite Instability
OXPHOS	Oxidative phosphorylation
PCA	Principal component analysis
TCGA	The Cancer Genome Atlas
TIL	Tumour-infiltrating lymphocyte
TME	Tumour microenvironment
Treg	Regulatory T cell
UMAP	Uniform Manifold Approximation and Projection

Authors:

Background

Colorectal cancer (CRC) is one of the most common malignancies of the digestive system. According to the latest global epidemiological statistics, CRC ranked as the third most frequently diagnosed cancer and the second leading cause of cancer-related death in both men and women worldwide in 2022[1].Advances in surgical techniques, radiochemotherapy, and targeted therapies have evolved the overall treatment paradigm for CRC, leading to improved local control and survival[2,3]. However, the drug resistance of colorectal cancer still limits the benefits that patients can obtain from the treatment[4].

The mechanisms of drug resistance mainly involve enhanced drug efflux, activation of DNA damage repair pathways, dysregulation of apoptosis, and maintenance of epithelial–mesenchymal transition (EMT). Concurrently, tumour-associated immunosuppression is mediated by tumour-associated macrophages (TAMs), regulatory T cells (Tregs), cancer-associated fibroblasts (CAFs), and aberrant activation of immune checkpoint signalling. These changes collectively contribute to therapeutic refractoriness in CRC. Understanding and reprogramming this suppressive network is therefore crucial for improving treatment responses[5–7]. The existence of drug resistance renders a substantial proportion of CRC patients unable to benefit from current regimens. Addressing this challenge requires an in-depth elucidation of the molecular mechanisms and cellular heterogeneity of the disease progression. Breakthrough insights in these areas will pave the way for the development of precision-guided therapeutic strategies to improve patient prognosis.

The advancement of genomic technology, particularly single-cell RNA sequencing (scRNA-seq), have provided powerful tools to dissect cellular diversity within the CRC microenvironment[8]. This approach enables high-resolution interrogation of gene expression profiles, uncovering the intricate mosaic of tumour, immune, and stromal cell populations—details that are often obscured in bulk tissue analyses[9]. These technologies have refined our understanding of disease architecture and have highlighted key molecular and cellular determinants underlying tumour progression, immune evasion, and therapeutic resistance. Analyzing the complex interactions among tumor cells, immune cells and stromal cells in the tumor microenvironment is of great significance for understanding the complexity of tumors and identifying potential disease and therapeutic targets[10].One of the major challenges in CRC management lies in elucidating the mechanisms of resistance. Using single-cell transcriptomic analyses, we identified a distinct epithelial subpopulation exhibiting drug-resistant features, and uncovered its key regulatory gene, providing new insights into therapeutic targets for resistant CRC.

TMEM184A (Transmembrane Protein 184 A)—a heparin-binding seven-pass transmembrane receptor—has drawn attention for its regulatory roles in vascular biology. TMEM184A mediates heparin-induced anti-inflammatory effects by promoting DUSP1 expression and suppressing JNK/p38 stress pathways; it also modulates cell proliferation and signalling in vascular smooth muscle and endothelial cells[11,12]. Its paralogue, TMEM184B, is markedly up-regulated in hypopharyngeal squamous cell carcinoma, where its knockdown reduces proliferation, migration, and invasion while enhancing apoptosis, suggesting a potential oncogenic role[13]. Multi-omics resources and the Human Protein Atlas further indicate that TMEM184A exhibits tissue-specific expression patterns across human organs and cancers[14].

In conclusion, the molecular mechanisms of treatment resistance in colorectal cancer (CRC) and the tumor microenvironment have not been fully elucidated. By integrating single-cell and bulk RNA sequencing data and further exploring the clinical relevance and prognosis of this gene based on clinical cases, this study systematically identified TMEM184A as a key gene driving CRC resistance and malignant progression. The aim of this research is to provide a theoretical basis for predicting specific biomarkers for resistant patients and improving the prognosis of patients with colorectal cancer.

Methods

Study design

This study employed a comprehensive multi-omics approach integrating single-cell RNA sequencing (scRNA-seq), bulk RNA sequencing, spatial transcriptomics, machine learning, and molecular docking to analyze the characteristics of colorectal cancer (CRC) cells and the intercellular networks. After drawing unique cell clusters

through single-cell analysis, we identified the drug-resistant subpopulations and used machine learning and transcriptomics analysis to screen out key genes. We first validated the candidate genes using publicly available transcriptomic datasets, and then performed immunohistochemical staining of the key genes in 180 paraffin-embedded colorectal cancer samples and their adjacent normal tissues to observe protein expression and analyze its correlation with clinical pathological features and prognosis, in order to explore the role of this protein in colorectal cancer patients. Finally, through drug sensitivity analysis and molecular docking, potential drugs and small molecule compounds targeting this protein were screened to provide a theoretical basis for clinical treatment.

Clinical data collection

We collected paraffin-embedded tissues and adjacent normal paraffin tissues from patients who underwent surgical resection for pathologically confirmed colorectal adenocarcinoma at Shanxi Cancer Hospital between January 2019 and June 2021. The patient cohort consisted of 102 males and 78 females, with ages ranging from 29 to 91 years and a median age of 63 years. Among these cases, 157 had complete clinical and pathological information.126 had complete follow-up information. Our inclusion criteria were as follows: (1) no preoperative antitumor treatment administered through any route; (2) complete clinical records available; (3) confirmation of adenocarcinoma through pathological examination of colorectal cancer biopsies and absence of tumor cell infiltration in the adjacent para-cancerous tissue.

Source of biological information data

All datasets used in this study were obtained from public database.scRNA-seq dataset: GSE161277 (healthy and tumour colorectal tissues; $n = 6$) was used to explore cellular heterogeneity within the tumour microenvironment. Spatial transcriptomics dataset: GSE226997, applied to validate spatial expression patterns of key genes and cell types.Microsatellite status dataset: GSE13294 (MSS vs. MSI; $n = 155$) for comparison of molecular differences between subtypes.Bulk RNA-seq dataset: The TCGA-COAD/READ cohort, comprising 571 CRC and 44 adjacent normal tissues (552 with complete clinical annotations), was used for machine learning, as well as survival and clinical association analyses.

Pre-processing of single-cell data and Seurat object construction

Data preprocessing was performed in R(4.3.1) using the Seurat (v5) package, which enables quality control, normalisation, and integration of scRNA-seq data.Expression matrices for all samples were imported and merged into a unified Seurat object. Quality control was conducted using three metrics: number of detected genes (nFeature_RNA), total RNA counts (nCount_RNA), and percentage of mitochondrial genes (percent_mt).Cells with > 25% mitochondrial reads or < 600 detected genes were removed. DoubletFinder was applied to identify and eliminate doublets. These steps ensured removal of low-quality or irrelevant cells, thereby minimising technical noise and improving biological accuracy[15,16].To correct for batch effects across samples, the SCTransform (SCT) workflow was used for data normalisation and integration, generating a high-quality expression matrix for downstream analyses.

Dimensionality reduction, clustering, and cell annotation

After data integration, Data were centred and scaled to remove depth- and batch-related biases, followed by Principal Component Analysis (PCA) for linear dimensionality reduction. The top 15 principal components (determined by the elbow plot) were retained for clustering.Cell clustering was performed using the FindNeighbors and FindClusters functions (resolution = 0.4). Marker genes for each cluster were identified with FindAllMarkers using the SCT-normalised matrix.Cell-type annotation was guided by PanglaoDB, the ACT online annotation platform, and published references to ensure biological reliability. The final major cell types included $CD4^+$ T cells, $CD8^+$ T cells, B cells, plasma cells, epithelial cells, fibroblasts, macrophages, NK cells, and dendritic cells.Non-linear dimensionality reduction and visualisation were performed using Uniform Manifold Approximation and Projection (UMAP) to depict cellular distributions and tumour–normal compositional differences.

Cell–cell communication analysis

Cell–cell communication networks were inferred using the CellChat package with the CellChatDB.human database as a reference for ligand–receptor interactions.Only significantly expressed ligand–receptor pairs were retained, and clusters with < 10 cells were excluded to reduce noise.This analysis systematically revealed intercellular signalling relationships and communication pathways, providing insights into the mechanisms of CRC cellular crosstalk.

Copy number variation (CNV) analysis

For epithelial tumour subclusters, Copy Number Variation (CNV) inference was conducted using CopyKAT to estimate chromosomal alterations based on scRNA-seq data. InferCNV was further used to identify segmental copy-number gains or losses across chromosomes, thereby characterising genomic heterogeneity and potential clonal architecture.Normal epithelial cells were used as a reference to ensure biological accuracy.

Pseudotime trajectory analysis

To reconstruct the developmental trajectories of epithelial tumour cells, representative normal epithelial clusters (based on marker expression and CNV profiles) were selected as the root state.Monocle3 was applied to perform pseudotime ordering, inferring the dynamic transition from normal to malignant phenotypes.The inferred pseudotime was mapped onto the UMAP embedding to visualise continuous transcriptional states

and transitional cell populations.This approach delineated epithelial heterogeneity and transcriptional evolution during CRC progression.

Functional and pathway activity scoring

To evaluate the pathway activity of different epithelial cell clusters, this study employed two scoring methods: (1) Using the MSigDB Hallmark gene set for AUCell analysis to investigate the pathway activity of each cell; (2) Employing the AddModuleScore function in combination with the drug resistance gene set to assess specific biological states. This revealed the pathway specificity and functional heterogeneity among different cell types.

Evaluating clinical significance through TCGA data

The prognostic relevance of marker genes derived from drug-resistant epithelial subclusters was evaluated in the TCGA CRC cohort.Patients were divided into high- and low-expression groups based on median gene expression levels.Kaplan–Meier (K–M) survival curves and log-rank tests assessed survival differences, while Cox proportional hazards regression estimated hazard ratios (HRs) and 95% confidence intervals.Associations between gene expression and TNM stage and clinical stage were further analysed.An integrated nomogram model combining gene expression and independent prognostic variables was constructed using the rms package to predict 1, 3, and 5-year survival probabilities.Model calibration was validated using bootstrap resampling, with calibration curves comparing predicted and observed survival.

Machine learning analysis

Two machine learning algorithms were applied to identify key prognostic genes: Least Absolute Shrinkage and Selection Operator (LASSO) regression, incorporating an L1 penalty for variable selection; andRandom Forest (RF), constructing ensemble decision-tree models and ranking variables by feature importance.These methods jointly identified genes with strong predictive value for survival outcomes.

Correlation analysis and protein–protein interaction (PPI) network

To explore co-expression patterns, genes significantly correlated with TMEM184A ($|\rho| \geq 0.4$, FDR < 0.05) were identified from the TCGA RNA-seq dataset.Protein–protein interaction (PPI) networks were then constructed using the STRING database and visualised in Cytoscape.Gene Ontology (GO) and KEGG pathway enrichment analyses were performed to elucidate biological processes (BP), molecular functions (MF), and cellular components (CC) associated with the correlated genes, thereby revealing key co-regulatory modules.

Comprehensive analysis of gene features

The mutation profiles of key genes were analyzed using the SangerBox platform (http://sangerbox.com). The correlations between gene expression, methylation levels and drug sensitivity were analyzed through the GSCA and CTR-DB 2.0 databases. The correlations between genes and immune infiltration were analyzed using the Cibersort、ssGSEA and Estimate algorithms.

Gene set enrichment analysis (GSEA)

GSEA was conducted to evaluate transcriptional differences between groups.Genes were ranked by expression fold change, and enrichment scores were calculated to identify up- or down-regulated pathways.Significant pathways were defined by FDR < 0.05 after permutation testing.

Tissue microarray preparation

A tissue microarray block instrument with a 2 mm aperture was used to create the paraffin microarray chip. A total of 180 colorectal cancer samples were re-evaluated based on hematoxylin–eosin stained (HE) sections, and the typical tumor areas were identified and marked on the pathological sections under a microscope. Using a puncture needle, the corresponding tissues marked on the HE sections were carefully picked and punched into the prepared blank tissue chip. Once the chips were prepared, they were placed upside down on the surface of a blank slide. Subsequently, the chips were heated at 55 °C in a drying oven for 7 min, followed by cooling down at room temperature outside the oven for 7 min. This heating and cooling process was repeated until the picked tissue was fully in contact with the paraffin on the chip[17].

Immunohistochemical staining

All tissue specimens were fixed in 10% neutral formalin, dehydrated in a gradient of alcohol, and then made transparent in xylene. Subsequently, the specimens were embedded in paraffin. The paraffin tissue microarrays used for immunohistochemical (IHC) staining had a thickness of 3 μm. For the automatic immunohistochemical staining, the Roche VENTANA BenchMark XT Immunohistochemical Stainer was employed. The rabbit anti-human TMEM184A polyclonal antibody (Catalog No.: 25989-1-AP, Proteintech Group, China) was diluted at a ratio of 1:200 in the antibody dilution. Other mediums and buffers were prepared as working solutions according to the requirements of the platform, with the exception of the primary TMEM184A antibody.

Interpretation of results

The localization of TMEM184A protein is mainly in the cytoplasm and the cell membrane.Positive TMEM184A staining was characterized by the presence of brownish-yellow granules in the cytoplasm and/or membrane of cancer cells. Two pathologists with over 10 years of experience conducted a double-blind test on the results of immunohistochemical staining. In cases of disagreement, a third pathologist re-evaluated the sections to determine a consensus score. The scoring system for TMEM184A immunostaining adopts the IRS (Immunoreactive Score) method, as defined below: The staining intensity is typically classified into four grades:

0 points: no positive staining, 1 point: light yellow, 2 points: brownish yellow, 3 points: brown. The proportion of positive cells is divided into four intervals: 1 point: <25% of cells are positive, 2 points: 25% – 50% of cells are positive, 3 points: 51% – 75% of cells are positive, 4 points: >75% of cells are positive. IRS = staining intensity × proportion of positive cells. A score of ≤ 6 points is defined as low expression, and > 6 points is defined as high expression.

Follow-up visit

The follow-up period commenced on the day of surgery, and the endpoint for the follow-up visit was either the date of the patient's death or June 30, 2025. Follow-up data of 126 cases were available for analysis. To assess the overall survival differences, a Kaplan–Meier overall survival curve was constructed.

Molecular docking analysis

The drug sensitivity characteristics of key genes were evaluated using the GSCA database, and potential drugs and small molecule compounds that could regulate gene expression were screened out. Chemical structure data were downloaded from the PubChem database and converted from SDF format to PDB format using the Open Babel software. The receptor protein structure data were sourced from the AlphaFold protein structure database (in PDB format). Protein processing (dehydration, hydrogenation, charge distribution) and molecular docking were completed in the AutoDock 4 software, and the ligands and receptors were converted to PDBQT format. The docking results were visualized and analyzed using PyMOL software to observe the interaction sites. A binding energy of <-5 kcal/mol was defined as having a good binding force.

Statistical analysis

Clinical pathological data analysis was conducted using SPSS 26.0 software. Qualitative variables were expressed by the number of cases, and inter-group comparisons were performed using McNemar test. Correlation analysis of clinical pathological features was conducted using χ^2 test. All other analyses were completed in R software (version 4.5.1). The Cox proportional hazards regression model was used to identify prognostic genes, and survival differences were evaluated using Kaplan-Meier (K-M) analysis. A P value < 0.05 was considered statistically significant.

Results

Single-cell transcriptome analysis of tumors and normal tissues

After quality control of the integrated single-cell dataset (Fig. 1A), dimensionality reduction was performed using principal component analysis (PCA). The first 15 principal components (determined by the elbow plot) were retained for downstream analyses, and clusters were visualised with UMAP. Cluster-specific marker genes were identified using FindAllMarkers (Fig. 1B), and the top 200 markers per cluster were subjected to Gene Ontology Biological Process (BP) enrichment (Fig. 1C). Manual cell-type annotation was guided by PanglaoDB, the ACT online resource and relevant literature, yielding UMAP maps for tumour versus normal samples (Fig. 1D). The annotations were further projected onto spatial transcriptomic sections (GSE226997) by deconvolution, confirming consistency and reliability (Fig. 1E).

Stacked bar plots showed marked differences in cellular composition between groups : epithelial cells were substantially enriched in tumours, whereas immune cells—particularly $CD8^+$T cells—were depleted(Fig. 1F). To probe putative intercellular mechanisms, CellChat was applied (Fig. 1G), revealing strongly enhanced epithelial signalling in tumours but reduced communication involving fibroblasts and $CD8^+$ T cells. The inter-group intensity comparison is presented through a differential heat map(Figure S1).

Identification of drug-resistant epithelial subtypes

To analyze epithelial heterogeneity, the epithelial cells from the tumor source were reclustered (Fig. 2A). The reliability of the clustering results was verified by the epithelial markers KRT8, KRT18, and EPCAM (Fig. 2B). For each epithelial subcluster, the top 200 marker genes were subjected to BP enrichment analysis. Subclusters 0–8 were mainly enriched in aerobic respiration, wound healing, cytoplasmic translation, viral process, aerobic electron transport chain, RNA splicing, Golgi vesicle transport, chromosome segregation, and DNA replication (Figure S2). Because copy-number variation (CNV) is a key mechanism conferring clonal advantage and driving tumour evolution, CopyKat was first used to infer chromosome-level CNVs with normal epithelium as reference (Fig. 2C). InferCNV then provided higher-resolution CNV profiling, showing that, except for cluster 4, most malignant epithelial subclusters harboured variable degrees of CNV (Fig. 2D). Notably, cluster 2 displayed widespread copy-number gains and losses, indicative of substantial genomic instability and a putative clonal selection advantage.

To infer differentiation dynamics, cluster 4 (normal-like by markers/CNV and functional context) was set as the root for Monocle3 pseudotime analysis, which was mapped back to UMAP space. Clusters 1 and 7 emerged as distinct termini(Fig. 2E)The BP enrichment analysis revealed that cluster 1 was enriched with features such as wound healing and actin filament tissues. Multiple studies have shown that actin filament organization is closely related to drug resistance[18–20]. In contrast, cluster 7 was enriched for chromosome segregation and mitotic nuclear division, reflecting high proliferation and anabolic metabolic activity (Figure S2). Notably, while Cluster 7 and Cluster 8 exhibited highly similar characteristics, including CNV patterns and Hallmark AUCell scores, Cluster 7 showed a significantly higher score in the G2M_CHECKPOINT pathway than Cluster 8. This suggests that Cluster 7 represents a specific functional subpopulation in a hyper-proliferative state. Retaining Cluster 7 as an independent cluster allows for the precise capture of the transition node from general proliferation to rapid proliferation, avoiding the loss of biological nuances related to cell cycle dynamics that might be obscured by over-integration.

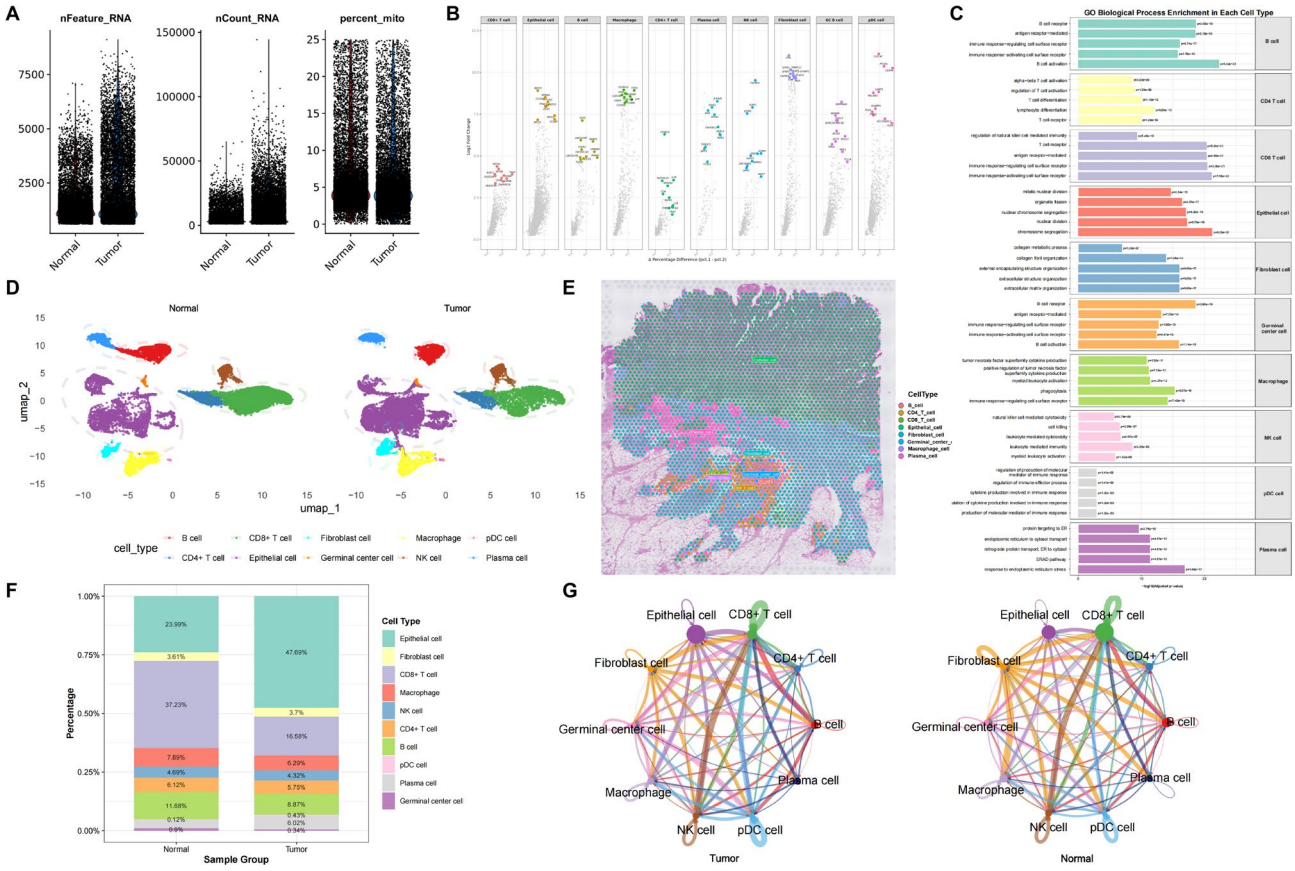

Fig. 1. Single-cell sequencing analysis of tumor and normal group samples. (**A**) Quality control plot of single-cell samples (percent mito > 25%, nFeature RNA < 600). (**B**) Top marker genes for each cell type. (**C**) BP enrichment analysis of the top 200 marker genes for each cell type. (**D**) UMAP dimensionality reduction plot for the normal and tumor groups (resolution = 0.4). (**E**) Single-cell annotation and deconvolution validated the accuracy of the annotation using colorectal cancer spatial transcriptomics slices. (**F**) Proportions of cell types in the tumor and normal groups. (**G**) Comparison of cell-cell communication intensity between the tumor and normal groups.

Hallmark AUCell scoring across malignant epithelial subclones (Fig. 2F) highlighted striking functional heterogeneity. Cluster 1 cell populations exhibit strong activation of the IFN-α/γ, TNF-α/NF-κB and TGF-β signaling pathways, accompanied by activation of the p53 pathway and hypoxia. In the tumor microenvironment, they are often reorganized to promote adaptive survival and treatment tolerance[21,22]. The synergistic TGF-β and hypoxia signals can induce epithelial-mesenchymal transition (EMT) and immune escape[23,24], while the tumor suppressor factor p53 can trigger tumor resistance to chemotherapy by maintaining genomic integrity[25]. Conversely, cluster 7 was dominated by cell-cycle control, DNA repair and metabolic reprogramming, with persistent MYC targets and mTORC1 activation consistent with anabolic growth[26,27].

The existing confirmed drug resistance genes[28–30] and immunosuppression genes[31–45] were queried in colorectal cancer. A customized gene set (Table S1) was created. Then, after scoring the epithelial cell clusters using the AddModuleScore function, it was shown that cluster 1 had the highest scores in terms of drug resistance and immunosuppression (Fig. 2G), indicating that the cells in this cluster exhibited stronger drug resistance and immunosuppressive properties. Based on CNV and trajectory context, cluster 1 may evolve from the highly unstable cluster 2, whereby heavy CNV burden fosters metastatic, drug-tolerant advantages[46–49].

It is worth noting that the drug resistance score of the cluster 6 is lower than that of the cluster 7. However, through the identification of high-variability genes, the cluster 6 was identified as goblet cells(Figure S3). Due to the significant differences in lineage origin and physiological function between goblet cells and the tumor cell subpopulation mainly derived from columnar epithelium, including it in the analysis might introduce interference signals related to cell differentiation. Therefore, following a comprehensive evaluation, the cluster 7 was selected for subsequent analysis due to its higher sensitivity to both chemotherapy and immunotherapy. Comparative cell–cell communication between the drug-resistant cell cluster 1 and the highly proliferative cell cluster 7 showed higher overall signalling activity in cluster 1. Multiple receptor–ligand axes were augmented in cluster 1—CEACAM1→CEACAM5, LAMB3→ITGA2/ITGB1, DSC2→DSG2, CDH1→CDH1, LAMB3→ITGA6/ITGB4, and MDK→NCL (Fig. 2H). The activation of the integrin axis indicates a stronger migration/invasion ability[50], and the enhancement of the MDK → NCL signaling pathway promotes the formation of an immunosuppressive microenvironment[51].Therefore, we have designated Cluster 1 as the primary focus for

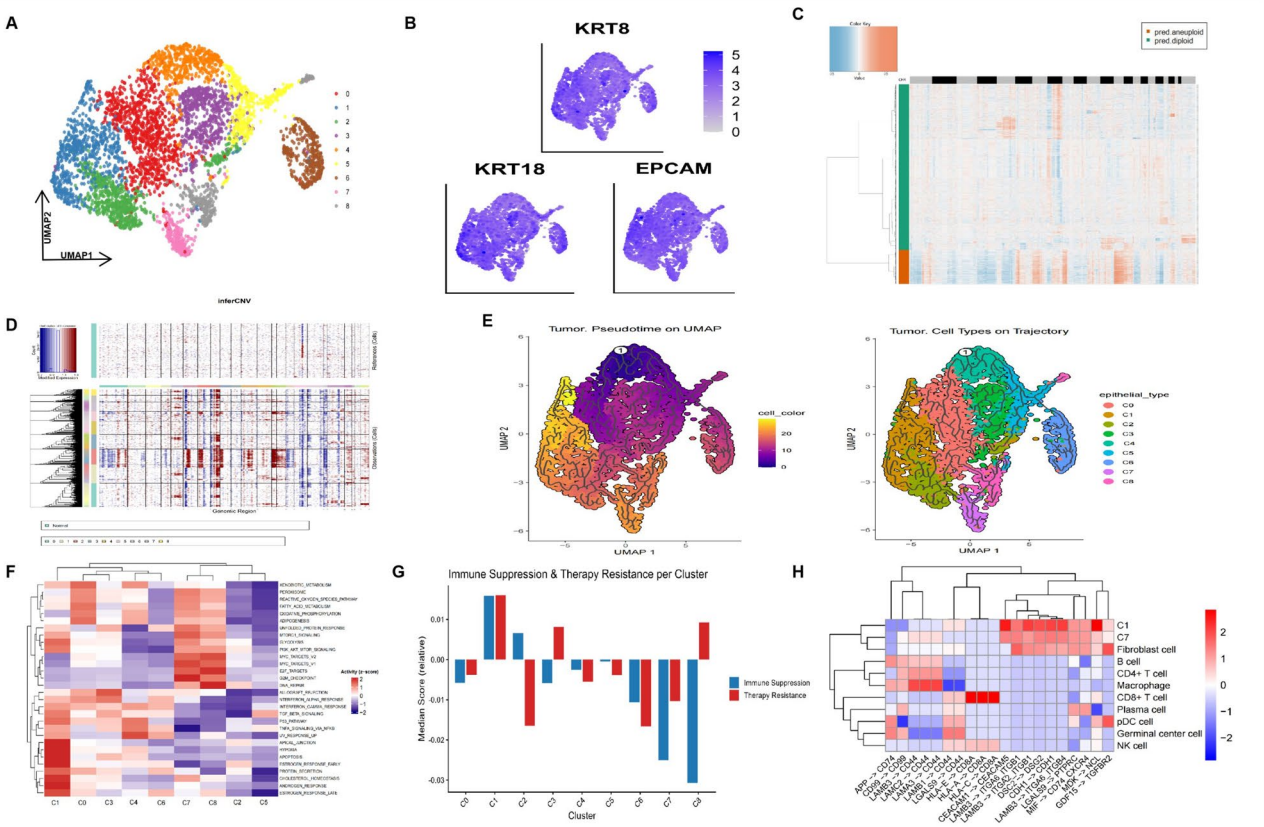

Fig. 2. Identification of drug resistance and immune suppression-related cell types. (**A**) UMAP plot of secondary clustering of epithelial cells, further divided into 9 subpopulations (resolution = 0.4). (**B**) Display of epithelial cell markers in the UMAP plot (KRT8/KRT18/EPCAM). (**C**) CopyKat analysis of copy number variations in epithelial cell types. (**D**) InferCNV analysis of copy number variations in epithelial cell types. (**E**) Pseudotime analysis of epithelial cells, showing two differentiation endpoints (C1 and C7, with C4 as the starting point). (**F**) AUCell scoring of epithelial cell types based on the MSigDB Hallmark gene set, with C1 and C7 enriched in distinct pathways. (**G**) Scoring of epithelial cell types using a custom drug resistance and immune suppression gene set via AddModuleScore, with C1 scoring significantly higher than other epithelial types. (**H**) Cell-cell communication analysis between C1/C7 epithelial cells and non-epithelial cells, with C1 showing higher activity.

investigating the mechanisms of drug resistance in colorectal cancer and for identifying potential therapeutic targets.

TMEM184A as a key gene in cluster 1

To explore the differences between drug-resistant cancer cell clusters and highly proliferative cancer cell clusters, and to screen key drug resistance genes, we conducted differential expression analysis on clusters 1 and 7. A total of 2,812 differentially expressed genes were identified (Fig. 3A), including 765 up-regulated genes and 2,047 down-regulated genes. In the TCGA colorectal cancer cohort, after conducting a survival analysis on 765 upregulated genes in cluster 1, a total of 57 prognostic genes were identified (Fig. 3B), among which 41 were classified as high-risk genes (hazard ratio HR > 1).To further screen out the key prognostic genes, the LASSO method (Figs. 3C-E) and the random forest method (Fig. 3F) were used to analyze 41 high-risk genes based on the survival outcome as the indicator; The intersection of the two models (Fig. 3G) yielded a total of five candidate genes: CTSD, HSPA1A, TMEM184A, IRF7 and FSTL3.

Membrane proteins are the key proteins for drug resistance. The transmembrane protein TMEM184A caught our attention. It is highly expressed in intestinal tissue[52]. Combined with subsequent bioinformatics analysis, it plays an important role in drug resistance and immune escape in colorectal cancer. Therefore, we finally determined it as a key gene driving drug resistance and conducted in-depth research on it. It is worth noting that this gene has not been studied in the context of cancer.

Expression profile and clinical significance of TMEM184A

GEPIA2 indicated significantly higher TMEM184A expression in CRC compared with normal tissues (Fig. 4A). GSCA methylation analysis showed hypomethylation of TMEM184A in CRC (Fig. 4B, C), consistent with

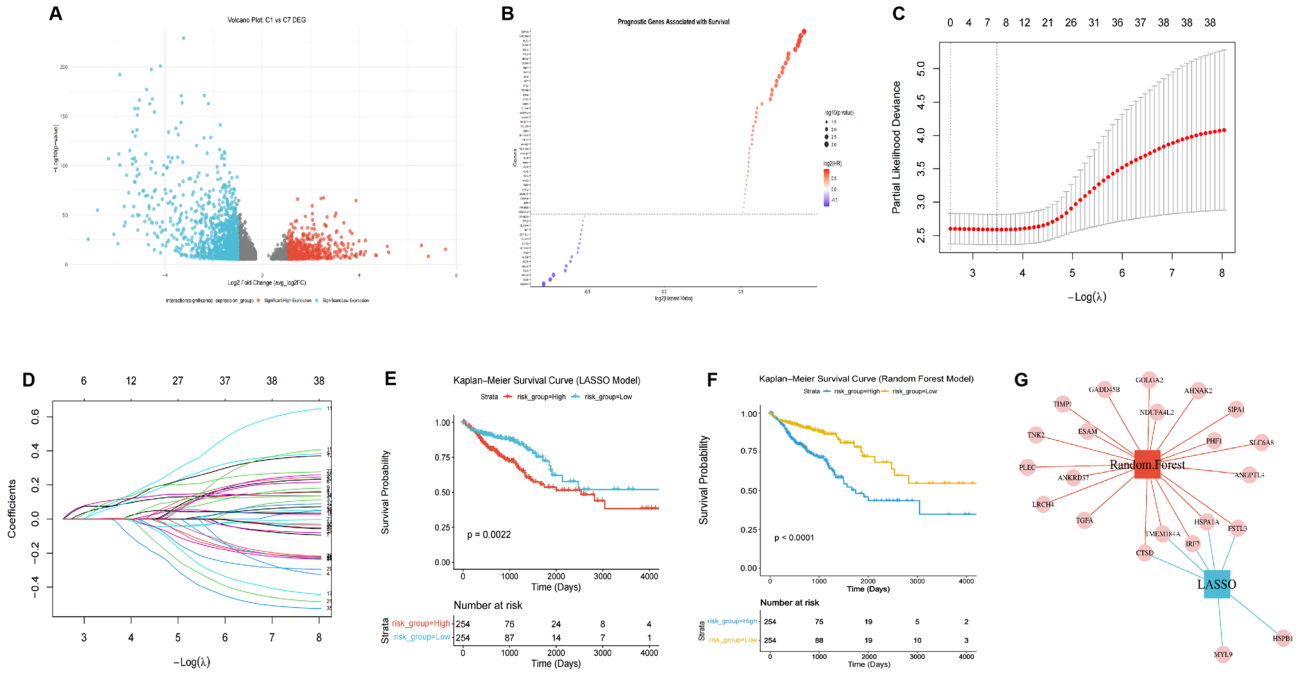

Fig. 3. Identification of TMEM184A as a key gene in C1. (**A**) Volcano plot of differential genes between C1 and C7(|logFC| > 1,P adj < 0.05). (**B**) Prognosis-related genes among the upregulated differential genes, with 41 high-risk genes (HR > 1). (**C**, **D**, and **E**) Lasso machine learning for the 41 high-risk genes to identify key genes. (**F**) Random forest machine learning for the 41 high-risk genes to identify key genes.G Intersection of key genes identified by Lasso and random forest machine learning.

epigenetic de-repression. Spatial transcriptomics (GSE226997) localised TMEM184A predominantly to epithelial cells (Fig. 4D).

In TCGA, higher TMEM184A expression associated with larger primary tumours (T), distant metastasis (M) and more advanced clinical stage, with an increasing trend across N stage despite non-significance (Fig. 4E). Kaplan–Meier analysis showed worse overall survival in the high-expression group(Fig. 4F). The nomogram and calibration curve constructed based on the multivariate Cox proportional hazards regression model indicate that TMEM184A can be regarded as an independent prognostic factor for patients with colorectal cancer. (Fig. 4G, H). Collectively, aberrant TMEM184A up-regulation aligns with adverse tumour biology.

Meanwhile, our analysis of the CTR-DB 2.0 (http://ctrdb.cloudna.cn/home) patient drug resistance database and the GEO (GSE173606) drug resistance cell dataset revealed that the expression level of TMEM184A was higher in the non-response group than in the response group(Figure S4). These data from clinical patient samples and drug-resistant cell lines consistently indicate that the high expression of TMEM184A is closely related to chemotherapy resistance in colorectal cancer.

Analysis of the TMEM184A regulatory network and associated genes

Correlation analysis in TCGA identified 469 genes significantly associated with TMEM184A expression. A STRING-based PPI network was constructed and visualized in Cytoscape to visually highlight the important genes. (Fig. 5A), alongside top positively correlated genes(Fig. 5B).

The GO/KEGG enrichment analysis of the top 200 positively correlated genes (Fig. 5C, D) revealed that they were significantly enriched in lipid metabolism pathways such as glycerol metabolism, glycerophospholipid metabolism, choline metabolism in cancer, and linoleic acid/α-linolenic acid metabolism[53–55]. This indicates that the TMEM184A transmembrane protein may promote cell resistance and invasion by regulating lipid metabolism on the membrane and receptor signal transduction.

The expression of TMEM184A is higher in MSS CRC

The GSCA database indicates that TMEM184A is significantly upregulated in MSS CRC(Fig. 6A), which was validated in GSE13294 (Fig. 6B). Prior studies show MSS CRC exhibits poor immunotherapy responsiveness relative to MSI disease[56,57] In the microsatellite stable colorectal cancer (GSE13294) samples, the samples were divided into high and low expression groups based on the median expression level of the TMEM184A gene, and GSEA enrichment analysis was performed. It was found that the high expression group of TMEM184A was significantly enriched in pathways related to fatty acid metabolism, oxidative phosphorylation, and exogenous metabolism (Fig. 6C), which was consistent with the previous results[58,59]. In summary, the research results indicate that TMEM184A can promote the treatment resistance of microsatellite stable colorectal cancer by driving metabolic reprogramming (especially fatty acid metabolism).

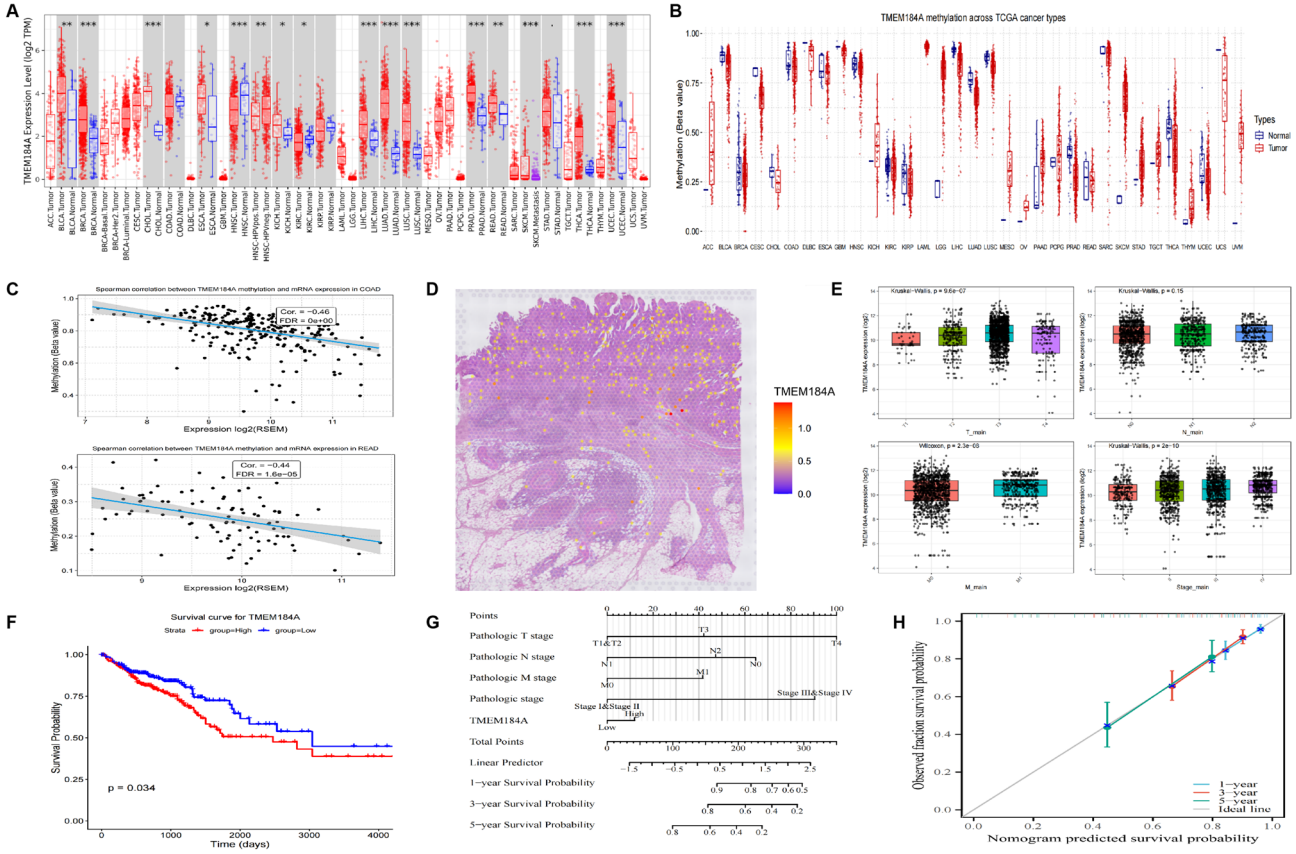

Fig. 4. Expression profile and clinical significance of TMEM184A. (**A**) TMEM184A is highly expressed in colorectal cancer (GEPIA2). (**B**) and (**C**) TMEM184A methylation level is reduced in colorectal cancer (GSCA), and its methylation level negatively correlates with TMEM184A expression. (**D**) TMEM184A is primarily expressed in epithelial cells in spatial transcriptomics slices. (**E**) High expression of TMEM184A is associated with T, M, and STAGE cancer staging. (**F**) High expression of TMEM184A is associated with poor prognosis. (**G**) Prognostic nomogram for TMEM184A, showing that its high expression decreases the 1-, 3-, and 5-year survival rates of CRC patients. (**H**) Prognostic calibration curve of TMEM184A confirming the accuracy of the nomogram model's prediction.

Immune infiltration and mutational landscape associated with TMEM184A

The deconvolution analysis based on Cibersort revealed that the increased expression of TMEM184A was positively correlated with regulatory T cells (Tregs) (R = 0.252) (Fig. 7A). Tregs can impair anti-tumor immunity and promote cancer progression by weakening the function of effector T cells (Teffs)[60]. Consistently, ESTIMATE revealed that TMEM184A-high CRC had lower ImmuneScore (R = − 0.371), StromalScore (R = − 0.261) and ESTIMATEScore (R = − 0.336)(Fig. 7B), indicating a "low-immune/low-stroma" state—an immune desert that facilitates immune evasion and progression. The stacked cibersort graph visualizes the changes in immune subpopulations between the high TMEM184A group and the low TMEM184A group at the sample level and between the groups (Fig. 7C).To further explore the relationship between TMEM184A and key immune cells within tumors, based on the TCGA colorectal cancer expression matrix, we divided the samples into high and low expression groups according to the median expression value of TMEM184A. Using the ssGSEA algorithm from the ImmuCellAI database (https://guolab.wchscu.cn/ImmuCellAI), we conducted an in-depth analysis of the correlation between TMEM184A and the tumor immune microenvironment. The results showed that high expression of TMEM184A significantly induced a phenotypic transformation of CRC from 'immune inflammatory type' to 'immune suppressive type'(Figure S5). Specifically, the proportions of antigen-presenting cells (DC) and effector killing cells (NK, $CD8^+$ T, Tc) that play a key role in anti-tumor function were significantly suppressed, and the synchronous decline of exhausted T cells (Tex) indicated that the mechanism was not inducing local exhaustion but rather an overall recruitment barrier, presenting a 'immune desertification' feature. This was corroborated by the ESTIMATE score of TMEM184A. At the same time, in the high-expression group of TMEM184A, the Treg subpopulation with strong immunosuppressive function (nTreg, iTreg) and the proportion of Th17 cells closely related to the malignant progression of CRC were significantly increased[61]. We speculate that this antagonistic pattern of "absence of killing cells" and "enrichment of inhibitory cells" promotes the poorer prognosis and low responsiveness to treatment in patients with high expression of TMEM184A. Mutation profilingshowed higher APC and TP53 mutation frequencies in TMEM184A-high tumours (Fig. 7D).

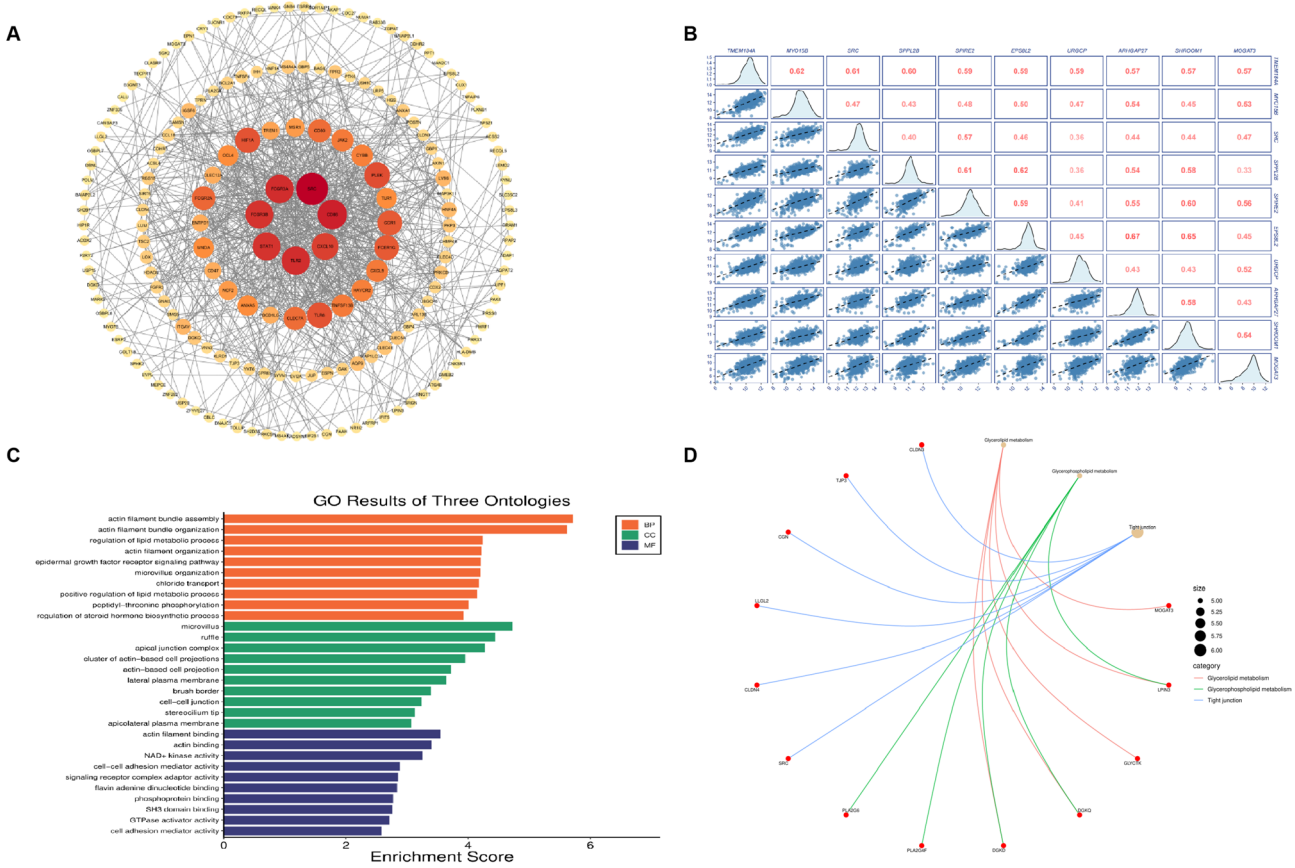

Fig. 5. TMEM184A regulatory network and analysis of related genes. (**A**) Protein-protein interaction network of TMEM184A-related genes, showing key modules of co-expressed genes. (**B**) Most significant positively correlated genes of TMEM184A. (**C**) GO enrichment analysis of the top 200 positively correlated genes of TMEM184A. (**D**) KEGG enrichment analysis of the top 200 positively correlated genes of TMEM184A.We have obtained formal permission from the copyright owner to use the results and images analyzed by KEGG.

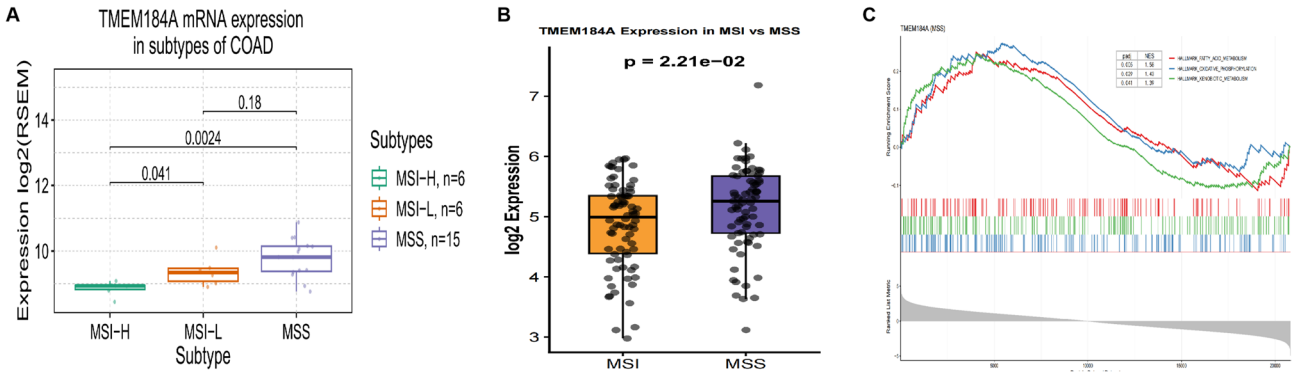

Fig. 6. High expression of TMEM184A in MSS-type colorectal cancer. (**A**) High expression of TMEM184A in MSS colorectal cancer (GSCA database). (**B**) High expression of TMEM184A in MSS colorectal cancer (GSE13294). (**C**) GSEA enrichment analysis of TMEM184A in MSS colorectal cancer (groups divided based on the median expression level of TMEM184A).

The clinical significance and prognosis of TMEM184A expression in colorectal cancer

To verify the results of the above bioinformatics analysis, we conducted an experimental test using paraffin-embedded tissue samples of colorectal cancer. We used immunohistochemical staining to detect the expression of TMEM184A protein in colorectal cancer tissues and paired normal tissues(Fig. 8A). The results showed that TMEM184A protein was mainly located in the cell membrane and cytoplasm. Compared with adjacent normal

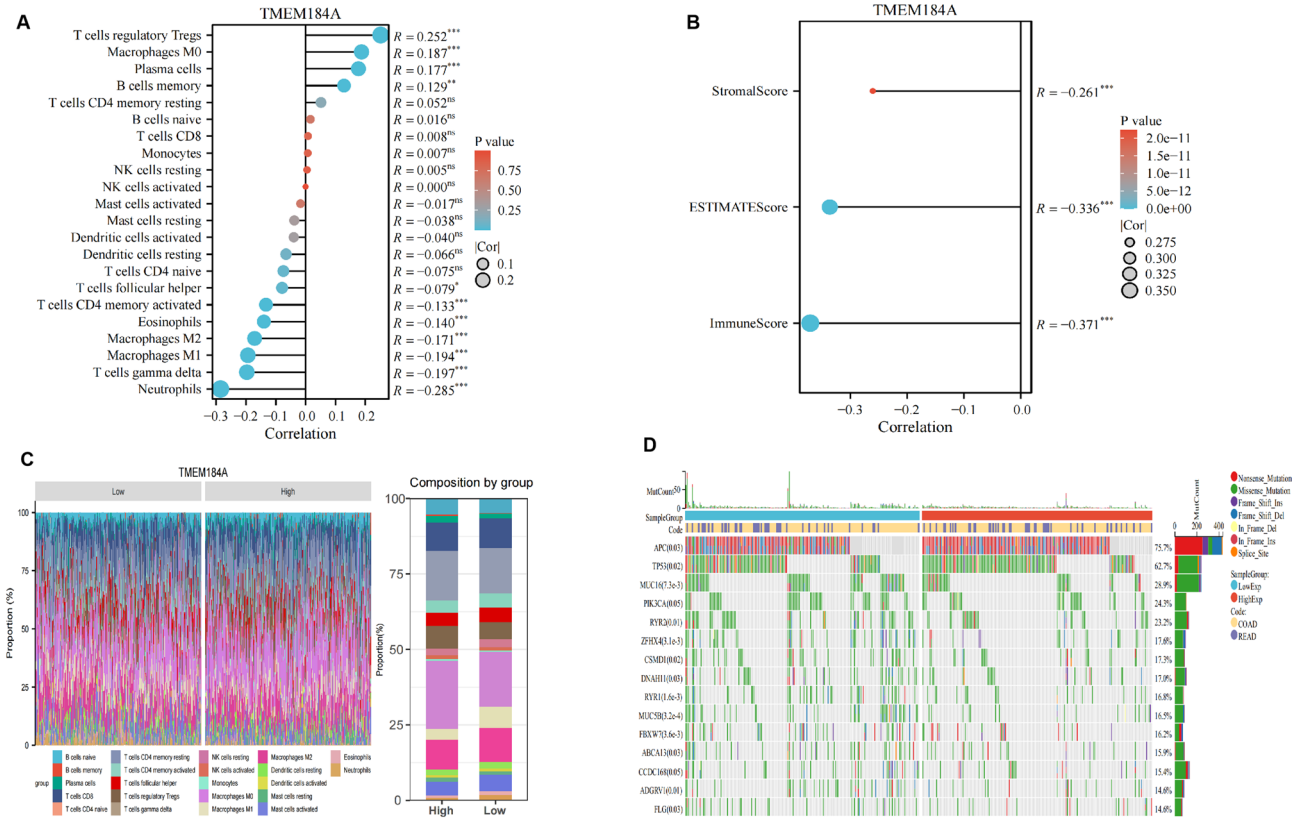

Fig. 7. Association analysis of TMEM184A expression with immune infiltration and mutation landscape. (**A**) Correlation between TMEM184A expression and immune cell infiltration. (**B**) Correlation between TMEM184A expression and immune score, stromal score, and overall score. (**C**) Stacked bar chart of immune cells in high and low TMEM184A expression groups. (**D**) Mutation landscape of high and low TMEM184A expression groups.

tissues, the high expression rate of TMEM184A protein in colorectal cancer tissues was higher (49.44%, 89 cases versus 35.56%, 64 cases. $P = 0.009$) (Table 1).

In addition, we also studied the relationship between TMEM184A expression and the clinical pathological characteristics of colorectal cancer patients. Based on the immunohistochemical results of TMEM184A, 157 colorectal cancer patients were divided into a low TMEM184A expression group (71 cases) and a high expression group (86 cases). The relationship between TMEM184A expression in colorectal cancer tissues and the clinical pathological characteristics of patients was analyzed. The results (Table 2) showed that high TMEM184A expression was related to lymph node metastasis and tumor location (high expression was more likely in the rectal region). However, TMEM184A expression level was not significantly associated with age, gender, degree of differentiation, TNM stage, stage, maximum tumor diameter, tumor type, tumor location, nerve invasion, vascular invasion, KRAS mutation, p53 mutation, and MSI status ($p > 0.05$). Stage was somewhat related to TMEM184A expression, although this association was not statistically significant ($p = 0.085$). In conclusion, the increase in TMEM184A expression in colorectal cancer is closely related to lymph node metastasis and tumor location (more likely to be highly expressed in the rectal region).

We generated a Kaplan-Meier survival curve for this cohort population to assess the impact of TMEM184A expression on the prognosis of colorectal cancer patients. The results showed that the 5-year overall survival rate of the high-expression group of TMEM184A was 64.71% (44 cases out of 68 cases), while that of the low-expression group was 81.03% (47 cases out of 58 cases), indicating that the prognosis of the high TMEM184A expression group was worse than that of the low-expression group ($p < 0.05$) (Fig. 8B). High TMEM184A expression was associated with poor prognosis in colorectal cancer patients, highlighting its potential as a prognostic biomarker in the treatment of colorectal cancer.

Drug screening targeting the TMEM184A protein

GSCA drug-sensitivity analyses suggested that higher TMEM184A is associated with reduced sensitivity to multiple chemotherapeutics(Fig. 9A, B), implying multidrug tolerance. Conversely, Cetuximab and several EGFR-family tyrosine kinase inhibitors (TKIs)—Afatinib, Lapatinib, Erlotinib, Gefitinib—appeared more effective in the TMEM184A-high context.To explore direct interactions, the AlphaFold model of TMEM184A (PDB) and PubChem ligand structures (SDF) were prepared (SDF→PDB via Open Babel), then processed for docking (dehydration, hydrogenation, charge assignment) and converted to PDBQT. AutoDock Vina docking

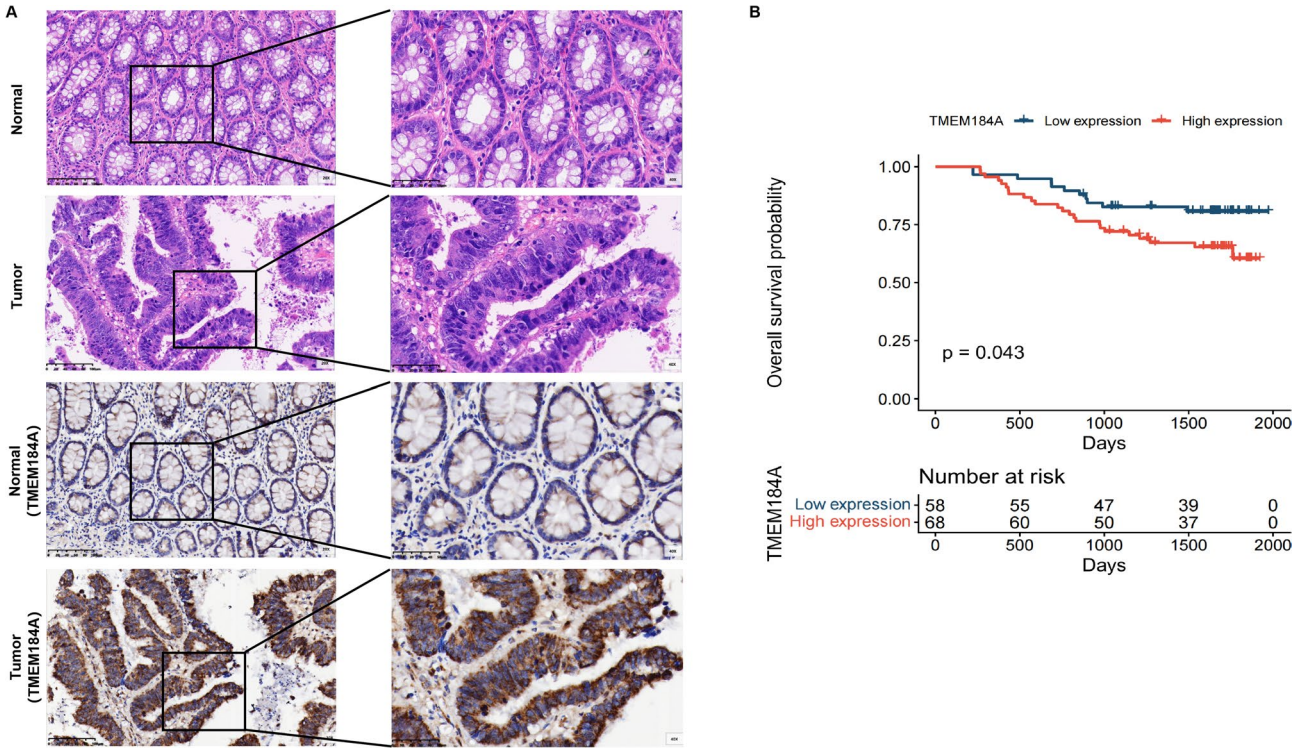

Fig. 8. A HE staining images of colorectal cancer and its adjacent tissues, as well as IHC TMEM184A staining images (200X and 400X). B The K-M survival curve (five-year overall survival rate) of the high and low expression groups of TMEM184A in 126 cases of colorectal cancer patients.

McNemar test	N High expression	N Low expression	Total
T High expression	34	55	89
T Low expression	30	61	91
Total	64	116	180
P	0.009		

Table 1. Tumor and normal group paired samples were tested using the McNemar test. The sample size was 180

and PyMOL visualisation indicated binding energies < − 5 kcal/mol for TMEM184A with Afatinib/Lapatinib/Erlotinib/Gefitinib, indicating that these drugs can inhibit the activation of the TMEM184A protein (Fig. 9C)[62].

By integrating GSCA with molecular docking technology, we propose that cetuximab and EGFR family tyrosine kinase inhibitors (TKIs) may antagonize the signal transduction mediated by TMEM184A protein by down-regulating or directly acting on this protein, thereby inhibiting the drug resistance and tumor malignant progression caused by high expression of TMEM184A.

Discussion

This study employed a multi-omics combined with clinical validation approach. Through single-cell omics analysis, it was discovered that the communication between tumor epithelial cells was more active than that of normal epithelial cells. In the tumor epithelial cells, we identified a drug-resistant subgroup, which exhibited high scores for chemotherapy resistance and immunosuppression. Temporal sequence analysis revealed that the drug-resistant subgroup and the high proliferation subgroup were two distinct differentiation endpoints. Through prognostic analysis and machine learning algorithms, the key marker TMEM184A of the drug-resistant subgroup was ultimately identified. Subsequently, We verified this result through the TCGA, GEO, CTR-DB 2.0 and GSCA databases as well as clinical samples, and confirmed that TMEM184A plays a promoting role in the progression of colorectal cancer.

Combined with GSEA enrichment analysis, our study indicates that TMEM184A can drive the therapeutic tolerance and malignant progression of colorectal cancer (especially microsatellite unstable colorectal cancer) by regulating the fatty acid metabolism pathway. And lipid metabolism reprogramming has been proven to promote chemotherapy resistance in cancer in previous studies[63]. Based on the lipid metabolism-related characteristics of TMEM184A, we speculate that it maintains receptor signal transduction and enhances drug resistance by

Clinicopathological features	TMEM184A			
	Low expression (n=58)	High expression (n=68)	χ^2	P
Age			0.161	0.689
≤55	17	23		
＞55	54	63		
Sex			0.793	0.373
Male	43	46		
Female	28	40		
Tumor differentiation			0.004	0.948
Well to Moderately differentiated	60	73		
Moderately to Poorly / Poorly differentiated	11	13		
Tumor location			3.988	0.046
Colon	25	18		
Rectum	46	48		
Vascular invasion			1.096	0.295
No	60	67		
Yes	11	19		
Perineural invasion			1.16	0.281
No	65	74		
Yes	6	12		
Tumor type			0.976	0.614
Polypoid type	7	10		
Ulcerative type	64	75		
Infiltrative type	0	1		
Maximum tumor diameter			0.037	0.847
≤4cm	44	52		
＞4cm	27	34		
T			0.112	0.737
T1-T2	19	21		
T3-T4	52	65		
N			4.653	0.031
N0	42	36		
N1-N2	29	50		
M			0.678	0.41
M0	70	83		
M1	1	3		
Stage				
I-II	42	39	2.968	0.085
III-IV	29	47		
Ki-67			0.103	0.748
≤60%	19	25		
＞60%	52	61		
P53				
Wild-type	25	33	0.167	0.683
Mutant	46	53		
MLH1			0.057	0.811
Negative	3	3		
Positive	68	83		
PMS2			0.057	0.811
Negative	3	3		
Positive	68	83		
MSH2			1.469	0.225
Negative	3	1		
Positive	68	85		
MSH6			0.455	0.5
Negative	3	2		
Continued				

Clinicopathological features	TMEM184A			
	Low expression (n=58)	High expression (n=68)	χ^2	P
Positive	68	84		
Microsatellite status			0.415	0.519
MSS	65	81		
MSI	6	5		

Table 2. The correlation between the high and low expression of TMEM184A and the clinical pathological characteristics of 157 colorectal cancer patients was analyzed using the chi-square test

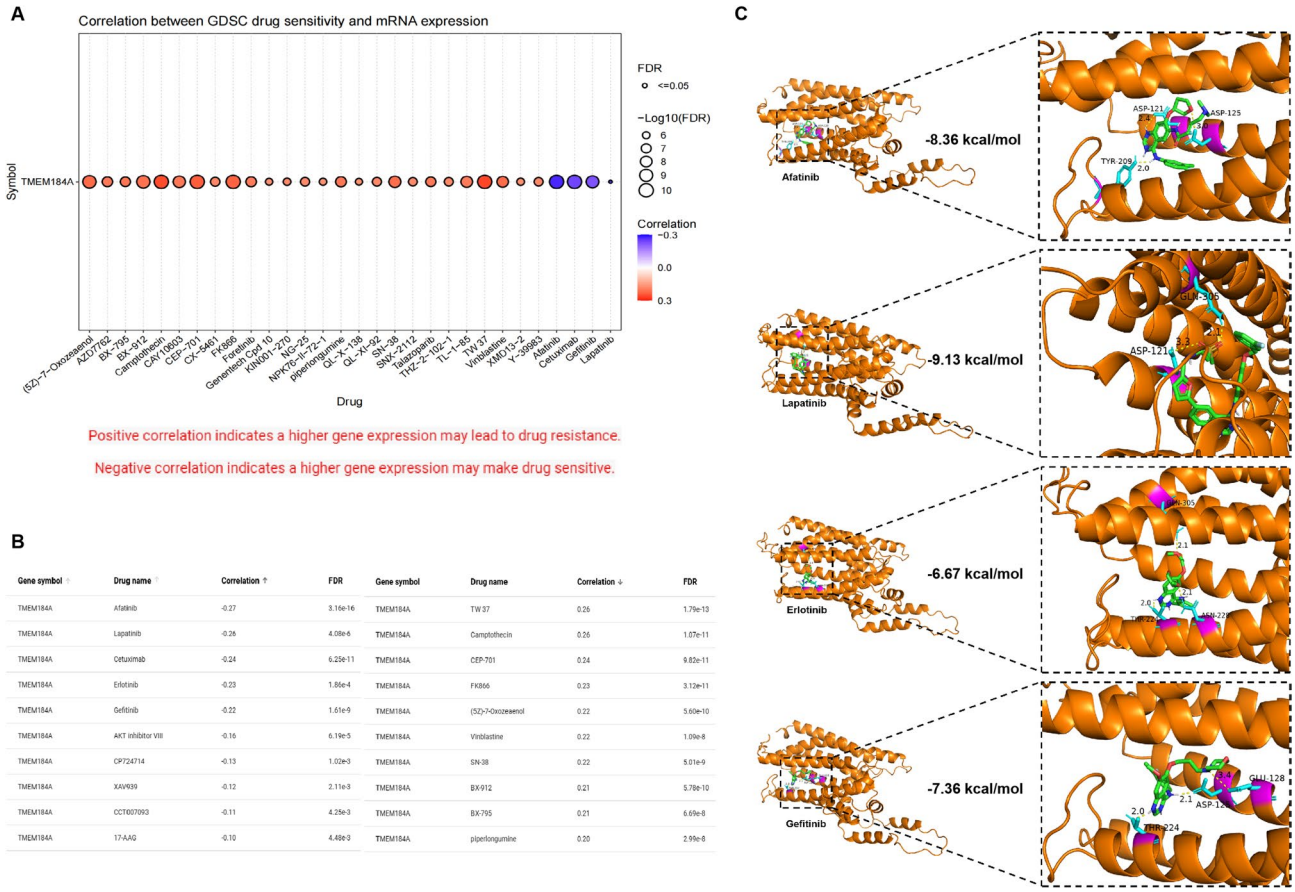

Gene symbol	Drug name	Correlation ↑	FDR
TMEM184A	Afatinib	-0.27	3.16e-16
TMEM184A	Lapatinib	-0.26	4.08e-6
TMEM184A	Cetuximab	-0.24	6.25e-11
TMEM184A	Erlotinib	-0.23	1.86e-4
TMEM184A	Gefitinib	-0.22	1.61e-9
TMEM184A	AKT inhibitor VIII	-0.16	6.19e-5
TMEM184A	CP724714	-0.13	1.02e-3
TMEM184A	XAV939	-0.12	2.11e-3
TMEM184A	CCT007093	-0.11	4.25e-3
TMEM184A	17-AAG	-0.10	4.48e-3

Gene symbol	Drug name	Correlation ↓	FDR
TMEM184A	TW 37	0.26	1.79e-13
TMEM184A	Camptothecin	0.26	1.07e-11
TMEM184A	CEP-701	0.24	9.82e-11
TMEM184A	FK866	0.23	3.12e-11
TMEM184A	(5Z)-7-Oxozeaenol	0.22	5.60e-10
TMEM184A	Vinblastine	0.22	1.09e-8
TMEM184A	SN-38	0.22	5.01e-9
TMEM184A	BX-912	0.21	5.78e-10
TMEM184A	BX-795	0.21	6.69e-8
TMEM184A	piperlongumine	0.20	2.99e-8

Fig. 9. Molecular docking of TMEM184A. (**A**) and (B) High expression of TMEM184A is associated with resistance to multiple drugs. (**C**) The TMEM184A protein shows good binding affinity with various EGFR family tyrosine kinase inhibitors.

reshaping the membrane lipid environment[64]. As far as we know, this is the first time that TMEM184A has been studied as a standalone potential biomarker in cancer.

From a clinical perspective, we analyzed the protein expression of TMEM184A in 180 paraffin samples from colorectal cancer patients using immunohistochemical methods. The protein expression of TMEM184A was significantly elevated in cancer tissues, and its high expression was associated with lymph node metastasis and tumor location. It was more prevalent in the rectal area, and its high expression was also related to the poor prognosis of colorectal cancer patients. Combined with drug sensitivity analysis and molecular docking results, TMEM184A has good binding characteristics with EGFR family tyrosine kinase inhibitors (such as afatinib, lapatinib), suggesting that this protein is located upstream or in a branch of the EGFR-related signaling pathway. It is notable that bioinformatics analysis showed that the expression of TMEM184A was higher in MSS colorectal cancer, which accounted for approximately 85% of colorectal cancers. These tumors have weak antigen presentation ability and limited response to immune checkpoint inhibitors (ICIs)[56], suggesting that the expression level of TMEM184A is related to the microsatellite status.In summary, TMEM184A plays a crucial role in drug resistance and the progression of colorectal cancer.

This study reveals the potential molecular mechanism by which TMEM184A drives drug resistance through fatty acid metabolism. Its high expression promotes lymph node metastasis and is associated with poor prognosis of colorectal cancer. TMEM184A can serve as a potential new biomarker for biological diagnosis. Additionally, molecular docking predicted that TMEM184A has a potential strong binding interaction with EGFR inhibitors such as Lapatinib. However, the mechanisms by which TMEM184A influences drug resistance through fatty acid metabolism, as well as the predicted drug interactions, require further validation through in vitro and in vivo drug sensitivity and functional experiment. In the future, we will conduct experiments to verify its molecular mechanism and drug sensitivity, thereby promoting clinical application.

Conclusions

TMEM184A, as a transmembrane protein, links the lipid metabolism pathway to the drug resistance of colorectal cancer. Its high expression is more prevalent in the rectal area and is associated with lymph node metastasis in patients with colorectal cancer. Moreover, its high expression is related to the poor prognosis of patients, with a lower 5-year survival rate. TMEM184A is expected to be a prognostic marker and therapeutic target for patients with drug-resistant colorectal cancer.

Data availability

GSE161277:Zheng X, Song J, Liu X, Yu C, Zhou Z, Shi H.Dissecting the Epithelial and Immune Evolution during Colorectal Carcinogenesis by Single-Cell RNA Sequencing.Gene Expression Omnibus.https:// identifiers. org/ geo: GSE161277 (2021)GSE226997:Park SS, Lee Y, Park S, Kim YH, Shin JS, Choi YW, Kim J, Park TJ. Visium Spatial transcriptomics analysis of human primary colorectal cancer. Gene Expression Omnibus.https:// identifiers. org/ geo: GSE226997 (2023).GSE13294:Ørntoft TF, Andersen CL. Expression data from primary colorectal cancers. Gene Expression Omnibus. https:// identifiers. org/ geo: GSE226997 (2009)GSE173606:Wu Q, Yao F, Wang Q, Xiang X.Non-coding RNA and mRNA expression profile in multi-drug resistance of colorectal cancer. Gene Expression Omnibus. https:// identifiers. org/ geo: GSE173606(2024)TCGA-COAD/READ: The Cancer Genome Atlas Network. Comprehensive molecular characterization of human colon and rectal cancer. The Cancer Genome Atlas. https://portal.gdc.cancer.gov/projects/TCGA-COAD & https://portal.gdc.cancer.gov/projects/TCGA-READ (2012)The bioinformatics codes and clinical information data used in this study can be obtained by the corresponding author upon reasonable request. The access to the clinical information data is restricted to non-commercial research purposes and the patient's sensitive information will be deleted.

Received: 15 January 2026; Accepted: 27 March 2026
Published online: 03 April 2026

References

1. Sung, H. et al. Global cancer statistics 2022: GLOBOCAN estimates of incidence and mortality worldwide for 36 cancers in 185 countries. *CA Cancer J. Clin.* **74** (3), 229–263. https://doi.org/10.3322/caac.21834 (2024).
2. NBenson, A. B. et al. Colon Cancer, Version 3.2024, NCCN Clinical Practice Guidelines in Oncology. *J. Natl. Compr. Canc Netw.* **22** (2 D), e240029. https://doi.org/10.6004/jnccn.2024.0029 (2024).
3. Benson, A. B. et al. NCCN Guidelines® Insights: Rectal Cancer, Version 3.2024. *J. Natl. Compr. Canc Netw.* **22** (6), 366–375. https://doi.org/10.6004/jnccn.2024.0041 (2024).
4. Zeng, K. et al. Inhibition of CDK1 Overcomes Oxaliplatin Resistance by Regulating ACSL4-mediated Ferroptosis in Colorectal Cancer. *Adv. Sci. (Weinh).* **10** (25), e2301088. https://doi.org/10.1002/advs.202301088 (2023).
5. Favier, S. et al. Exploring and bypassing resistance to targeted therapies in colorectal cancer. *Biomed. Pharmacother.* **193**, 118741. https://doi.org/10.1016/j.biopha.2025.118741 (2025).
6. O'Connor, M. J. Targeting the DNA Damage Response in Cancer. *Mol. Cell.* **60** (4), 547–560. https://doi.org/10.1016/j.molcel.2015.10.040 (2015).
7. Kennel, K. B. & Greten, F. R. The immune microenvironment of colorectal cancer. *Nat. Rev. Cancer.* **25** (12), 945–964. https://doi.org/10.1038/s41568-025-00872-1 (2025).
8. Ziegenhain, C. et al. Comparative Analysis of Single-Cell RNA Sequencing Methods. *Mol. Cell.* **65** (4), 631–643e4. https://doi.org/10.1016/j.molcel.2017.01.023 (2017).
9. Papalexi, E. & Satija, R. Single-cell RNA sequencing to explore immune cell heterogeneity. *Nat. Rev. Immunol.* **18** (1), 35–45. https://doi.org/10.1038/nri.2017.76 (2018).
10. Tirosh, I. et al. Dissecting the multicellular ecosystem of metastatic melanoma by single-cell RNA-seq. *Science* **352** (6282), 189–196. https://doi.org/10.1126/science.aad0501 (2016).
11. Pugh, R. J. et al. Transmembrane Protein 184A Is a Receptor Required for Vascular Smooth Muscle Cell Responses to Heparin. *J. Biol. Chem.* **291** (10), 5326–5341. https://doi.org/10.1074/jbc.M115.681122 (2016).
12. Farwell, S. L. et al. Heparin Decreases in Tumor Necrosis Factor α (TNFα)-induced Endothelial Stress Responses Require Transmembrane Protein 184A and Induction of Dual Specificity Phosphatase 1. *J. Biol. Chem.* **291** (10), 5342–5354. https://doi.org/10.1074/jbc.M115.681288 (2016).
13. Lin, Y. et al. TMEM184B promotes proliferation, migration and invasion, and inhibits apoptosis in hypopharyngeal squamous cell carcinoma. *J. Cell. Mol. Med.* **26** (21), 5551–5561. https://doi.org/10.1111/jcmm.17572 (2022).
14. Uhlén, M. et al. Tissue-based map of the human proteome. *Science* **347** (6220), 1260419. https://doi.org/10.1126/science.1260419 (2015).
15. Hao, Y. et al. Integrated analysis of multimodal single-cell data. *Cell* **184** (13), 3573–3587e29. https://doi.org/10.1016/j.cell.2021.04.048 (2021).
16. McGinnis, C. S., Murrow, L. M., Gartner, Z. J. & DoubletFinder Doublet Detection in Single-Cell RNA Sequencing Data Using Artificial Nearest Neighbors. *Cell. Syst.* **8** (4), 329–337e4. https://doi.org/10.1016/j.cels.2019.03.003 (2019).
17. Cui, W. et al. Exploring the expression and clinical significance of the miR-140-3p-HOXA9 axis in colorectal cancer. *J. Cancer Res. Clin. Oncol.* **150** (2), 47. https://doi.org/10.1007/s00432-023-05592-3 (2024).
18. Shimizu, T., Fujii, T. & Sakai, H. The Relationship Between Actin Cytoskeleton and Membrane Transporters in Cisplatin Resistance of Cancer Cells. *Front. Cell. Dev. Biol.* **8**, 597835. https://doi.org/10.3389/fcell.2020.597835 (2020).
19. Su, L. et al. Disruption of the association between drug transporter and actin cytoskeleton abolishes drug resistance in hypertrophic scar. *Oncotarget* **8** (2), 2617–2627. https://doi.org/10.18632/oncotarget.13734 (2017).

20. Kim, M. H. et al. Actin remodeling confers BRAF inhibitor resistance to melanoma cells through YAP/TAZ activation. *EMBO J.* **35** (5), 462–478. https://doi.org/10.15252/embj.201592081 (2016).
21. Ahn, K. S., Sethi, G. & Aggarwal, B. B. Reversal of chemoresistance and enhancement of apoptosis by statins through down-regulation of the NF-kappaB pathway. *Biochem. Pharmacol.* **75** (4), 907–913. https://doi.org/10.1016/j.bcp.2007.10.010 (2008).
22. López-Soto, A., Gonzalez, S. & Folgueras, A. R. IFN Signaling and ICB Resistance: Time is on Tumor's Side. *Trends Cancer.* **3** (3), 161–163. https://doi.org/10.1016/j.trecan.2017.01.004 (2017).
23. Park, J. et al. TGF-β1 and hypoxia-dependent expression of MKP-1 leads tumor resistance to death receptor-mediated cell death. *Cell. Death Dis.* **4** (2), e521. https://doi.org/10.1038/cddis.2013.42 (2013).
24. Luo, W. et al. TGF-β-driven EMT in cancer progression and drug resistance. *Cytokine Growth Factor. Rev.* **85**, 11–25. https://doi.org/10.1016/j.cytogfr.2025.05.004 (2025).
25. Cao, M. et al. p53 activates circASCC3 to repress R-loops and enhance resistance to chemotherapy. *Proc. Natl. Acad. Sci. U S A.* **122** (11), e2415869122. https://doi.org/10.1073/pnas.2415869122 (2025).
26. Joshi, J. N. et al. mTORC1 activity oscillates throughout the cell cycle, promoting mitotic entry and differentially influencing autophagy induction. *Cell. Rep.* **43** (8), 114543. https://doi.org/10.1016/j.celrep.2024.114543 (2024).
27. Zhang, Y. & Dong, F. Gfi1 upregulates c-Myc expression and promotes c-Myc-driven cell proliferation. *Sci. Rep.* **10** (1), 17115. https://doi.org/10.1038/s41598-020-74278-4 (2020).
28. Wang, Q. et al. Drug Resistance in Colorectal Cancer: From Mechanism to Clinic. *Cancers (Basel).* **14** (12), 2928. https://doi.org/10.3390/cancers14122928 (2022).
29. Sreekumar, R. et al. The ZEB2-dependent EMT transcriptional programme drives therapy resistance by activating nucleotide excision repair genes ERCC1 and ERCC4 in colorectal cancer. *Mol. Oncol.* **15** (8), 2065–2083. https://doi.org/10.1002/1878-0261.12965 (2021).
30. Zhou, J. et al. The Drug-Resistance Mechanisms of Five Platinum-Based Antitumor Agents. *Front. Pharmacol.* **11**, 343. https://doi.org/10.3389/fphar.2020.00343 (2020).
31. Dong, H. et al. Tumor-associated B7-H1 promotes T-cell apoptosis: a potential mechanism of immune evasion. *Nat. Med.* **8** (8), 793–800. https://doi.org/10.1038/nm730 (2002).
32. Latchman, Y. et al. PD-L2 is a second ligand for PD-1 and inhibits T cell activation. *Nat. Immunol.* **2** (3), 261–268. https://doi.org/10.1038/85330 (2001).
33. Wu, F. et al. HHLA2 promotes immune evasion in EGFR-mutant lung cancer by inhibiting CD8 + T cell glutamine metabolism via KIR3DL3 interaction. *Cancer Lett.* **639**, 218219. https://doi.org/10.1016/j.canlet.2025.218219 (2025).
34. Hussein, O. J. et al. The role of immune checkpoints in modulating cancer stem cells anti-tumor immune responses: implications and perspectives in cancer therapy. *J. Exp. Clin. Cancer Res.* **44** (1), 305. https://doi.org/10.1186/s13046-025-03514-4 (2025).
35. Li, T. J. et al. SIGLEC15 amplifies immunosuppressive properties of tumor-associated macrophages in pancreatic cancer. *Cancer Lett.* **530**, 142–155. https://doi.org/10.1016/j.canlet.2022.01.026 (2022).
36. de Oliveira, P. H. S., Silva-Freitas, B. B. & Meyer-Fernandes, J. R. Hypoxia as a Central Regulator of Plasma Membrane Phosphohydrolase Enzymes: Possible Roles in Extracellular Phosphate Generation and Adenosine Metabolism. *Membr. (Basel).* **15** (12), 381. https://doi.org/10.3390/membranes15120381 (2025).
37. Nikolić, N. et al. Oral Microbiota and Carcinogenesis: Exploring the Systemic Impact of Oral Pathogens. *Pathogens* **14** (12), 1233. https://doi.org/10.3390/pathogens14121233 (2025).
38. Ye, J. et al. Targeting the CD47-HCK-LGALS9 axis disrupts proliferation-immunosuppression coupling in early-stage endometrial cancer. *Mol. Cancer.* (2025). https://doi.org/10.1186/s12943-025-02534-0
39. Nan, L. et al. Harnessing the innate immune system: a novel bispecific antibody targeting CD47 and CD24 for selective tumor clearance. *J. Immunother Cancer.* **13** (12), e013283. https://doi.org/10.1136/jitc-2025-013283 (2025).
40. Beli, X. et al. Harnessing the immunomodulatory properties of HLA-G for advanced immunotherapies. *Front. Immunol.* **16**, 1716778. https://doi.org/10.3389/fimmu.2025.1716778 (2025).
41. Mezrich, J. D. et al. An interaction between kynurenine and the aryl hydrocarbon receptor can generate regulatory T cells. *J. Immunol.* **185** (6), 3190–3198. https://doi.org/10.4049/jimmunol.0903670 (2010).
42. Deng, Z. et al. TGF-β signaling in health, disease, and therapeutics. *Signal. Transduct. Target. Ther.* **9** (1), 61. https://doi.org/10.1038/s41392-024-01764-w (2024).
43. Hong, S. et al. Exploration of the roles of CAFs in melanoma based on single-cell transcriptomics and spatial transcriptomics. *Discov Oncol.* **16** (1), 2105. https://doi.org/10.1007/s12672-025-03868-3 (2025).
44. Santibanez, J. F. Myeloid-Derived Suppressor Cells: Implications in Cancer Immunology and Immunotherapy. *Front. Biosci. (Landmark Ed).* **30** (3), 25203. https://doi.org/10.31083/FBL25203 (2025).
45. Wu, B., Zhang, B., Li, B., Wu, H. & Jiang, M. Cold and hot tumors: from molecular mechanisms to targeted therapy. *Signal. Transduct. Target. Ther.* **9** (1), 274. https://doi.org/10.1038/s41392-024-01979-x (2024).
46. Davoli, T. et al. Tumor aneuploidy correlates with markers of immune evasion and with reduced response to immunotherapy. *Science* **355** (6322), eaaf8399. https://doi.org/10.1126/science.aaf8399 (2017).
47. Bielski, C. M. et al. Genome doubling shapes the evolution and prognosis of advanced cancers. *Nat. Genet.* **50** (8), 1189–1195. https://doi.org/10.1038/s41588-018-0165-1 (2018).
48. Chen, M., Linstra, R. & van Vugt, M. A. T. M. Genomic instability, inflammatory signaling and response to cancer immunotherapy. *Biochim. Biophys. Acta Rev. Cancer.* **1877** (1), 188661. https://doi.org/10.1016/j.bbcan.2021.188661 (2022).
49. Lee, A. J. et al. Chromosomal instability confers intrinsic multidrug resistance. *Cancer Res.* **71** (5), 1858–1870. https://doi.org/10.1158/0008-5472.CAN-10-3604 (2011).
50. Desgrosellier, J. S. & Cheresh, D. A. Integrins in cancer: biological implications and therapeutic opportunities. *Nat. Rev. Cancer.* **10** (1), 9–22. https://doi.org/10.1038/nrc2748 (2010).
51. Yu, X. et al. Integrating single-cell RNA-seq and spatial transcriptomics reveals MDK-NCL dependent immunosuppressive environment in endometrial carcinoma. *Front. Immunol.* **14**, 1145300. https://doi.org/10.3389/fimmu.2023.1145300 (2023).
52. Ji, Z. et al. Molecular characterization of vascular intestinal obstruction using whole-exome sequencing. *Ann. Transl Med.* **10** (8), 442. https://doi.org/10.21037/atm-22-1134 (2022).
53. Kanehisa, M., Furumichi, M., Sato, Y., Matsuura, Y. & Ishiguro-Watanabe, M. KEGG: biological systems database as a model of the real world. *Nucleic Acids Res.* **53** (D1), D672–D677. https://doi.org/10.1093/nar/gkae909 (2025).
54. Kanehisa, M. Toward understanding the origin and evolution of cellular organisms. *Protein Sci.* **28** (11), 1947–1951. https://doi.org/10.1002/pro.3715 (2019).
55. Kanehisa, M. & Goto, S. KEGG: kyoto encyclopedia of genes and genomes. *Nucleic Acids Res.* **28** (1), 27–30. https://doi.org/10.1093/nar/28.1.27 (2000).
56. Guven, D. C. et al. The Efficacy of Immune Checkpoint Inhibitors in Microsatellite Stable Colorectal Cancer: A Systematic Review. *Oncologist* **29** (5), e580–e600. https://doi.org/10.1093/oncolo/oyae013 (2024).
57. Ros, J. et al. Advances in immune checkpoint inhibitor combination strategies for microsatellite stable colorectal cancer. *Front. Oncol.* **13**, 1112276. https://doi.org/10.3389/fonc.2023.1112276 (2023).
58. Li, B., Mi, J. & Yuan, Q. Fatty acid metabolism-related enzymes in colorectal cancer metastasis: from biological function to molecular mechanism. *Cell. Death Discov.* **10** (1), 350. https://doi.org/10.1038/s41420-024-02126-9 (2024).
59. Chen, X. et al. The effects of metabolism on the immune microenvironment in colorectal cancer. *Cell. Death Discov.* **10** (1), 118. https://doi.org/10.1038/s41420-024-01865-z (2024).

60. Zhang, A. et al. Regulatory T cells in immune checkpoint blockade antitumor therapy. *Mol. Cancer.* **23** (1), 251. https://doi.org/10.1186/s12943-024-02156-y (2024).
61. Liu, X. et al. Th17 Cells Secrete TWEAK to Trigger Epithelial-Mesenchymal Transition and Promote Colorectal Cancer Liver Metastasis. *Cancer Res.* **84** (8), 1352–1371. https://doi.org/10.1158/0008-5472.CAN-23-2123 (2024).
62. Trott, O. & Olson, A. J. AutoDock Vina: improving the speed and accuracy of docking with a new scoring function, efficient optimization, and multithreading. *J. Comput. Chem.* **31** (2), 455–461. https://doi.org/10.1002/jcc.21334 (2010).
63. Cao, Y. Adipocyte and lipid metabolism in cancer drug resistance. *J. Clin. Invest.* **129** (8), 3006–3017. https://doi.org/10.1172/JCI127201 (2019).
64. Beloribi-Djefaflia, S., Vasseur, S. & Guillaumond, F. Lipid metabolic reprogramming in cancer cells. *Oncogenesis* **5** (1), e189. https://doi.org/10.1038/oncsis.2015.49 (2016).

Acknowledgements
We gratefully acknowledge the use of data and resources provided by GEO, TCGA, SangerBox Platform, GEPIA2, GSCA, PubChem, CTR-DB 2.0, ImmuCellAI and AlphaFold. Their support has been essential to the completion of this work.

Author contributions
YX, YC, and XB designed the project; XB is responsible for bioinformatics analysis and statistical analysis; PB, RL and GZ are responsible for the immunohistochemical staining experiment; ZB, PB and GZ participated in discussions and promoted the progress of the project; XB, ZB and WC jointly wrote the manuscript. All authors read and approved the final manuscript.

Funding
This work received funding support from the National Natural Science Foundation of China (Grant number: 82172659).

Declarations

Ethics approval and consent to participate
This study was performed in line with the principles of the Declaration of Helsinki. Approval was granted by the Ethics Committee of Shanxi Provincial Cancer Hospital (No.202112).

Consent for publication
Informed consent was obtained from all individual participants included in the study.

Competing interests
The authors declare no competing interests.

Additional information
Supplementary Information The online version contains supplementary material available at https://doi.org/10.1038/s41598-026-46674-9.

Correspondence and requests for materials should be addressed to Y.C. or Y.X.